Send Orders for Reprints to reprints@benthamscience.net

RESEARCH ARTICLE

Antioxidant and Antiangiogenic Effect of Homoleptic Palladium (II) Carboxamide Complex Loaded Chitosan Modified PLGA Nanoparticles: *In vitro* Evaluation and *In vivo* Chick Embryo Chorioallantoic Membrane (CAM) Assay

A. Alper Öztürk[1,*], Hakan Ünver[2] and H. Tuba Kıyan[3]

[1]*Department of Pharmaceutical Technology, Faculty of Pharmacy, Anadolu University, Eskişehir, Türkiye;* [2]*Department of Chemistry, Faculty of Science, Eskisehir Technical University, Eskişehir, Türkiye;* [3]*Department of Pharmacognosy, Faculty of Pharmacy, Anadolu University, Eskişehir, Türkiye*

ARTICLE HISTORY

Received: September 15, 2022
Revised: February 03, 2023
Accepted: February 07, 2023

DOI:
10.2174/1570180820666230214091500

This is an Open Access article published under CC BY 4.0 https://creativecommons.org/licenses/by/4.0/legalcode

Abstract: ***Background*:** Angiogenesis is a natural and complex mechanism that is regulated by biomolecules formed by the body. Medicinal inorganic chemistry is increasing in popularity due to metal-based compounds, offering significant chances and possibilities for building novel anti-cancer medicines with promising anti-angiogenic effects.

***Objective*:** This study aimed to examine the successful results obtained from treatments with nanoparticle formulations of active drug substances.

***Methods*:** The nanoprecipitation/solvent displacement approach, with some changes, was used to make PLGA-based NPs.

***Result*:** The particle size obtained in the blank formulation was 82.4-473.9 nm, while the particle size in the API-loaded NPs was 193.2-678.0 nm. Among the formulations, NP-950-P, NP-390-P, and NP-350-CSP2 were found to have significant antioxidant potentials with IC_{50} values of 3.025, 5.198, and 7.4242 $\mu g.mL^{-1}$, respectively, when compared to Vit C. According to the microscopic evaluations, NP-950-P (including $Pd(PyCrbx)_2Cl_2$ as 50 $\mu g.pellet^{-1}$) and NP-950-CSP2 (including $Pd(PyCrbx)_2Cl_2$ as 50 $\mu g.pellet^{-1}$) showed strong anti-angiogenic effect whereas the other NP formulations showed weak anti-angiogenic effect when compared with the positive control (±)-Thalidomide at the concentration of 50 $\mu g.pellet^{-1}$.

***Conclusion*:** When the results were examined, it was found that nanoscale drug carrier systems were prepared, and high antioxidant activity and anti-angiogenesis activity were detected, especially in nanoparticles prepared with 950. As per our knowledge, it is the first study in this field that will bring a new perspective to cancer treatment.

Keywords: Nanoparticle, PLGA, chitosan, cancer, CAM, angiogenesis, palladium, carboxamide.

1. INTRODUCTION

Cancer has long been one of the leading causes of death worldwide [1]. Cancer can be defined as uncontrolled cell proliferation. The most important feature of cancer is abnormal cell divisions that occur in various parts of the body and can spread to other organs [2]. As the world population ages, the number of older people with cancer is expected to increase. Although cancer affects people of all ages, patients aged 70 and over account for 42% of all cancer patients [3]. Cancer continues to be a significant health and social problem. According to the World Health Organization (WHO), the global cancer burden increased last year and is currently at its highest, with 18.1 million new cases and 9.6 million cancer deaths. Despite increased financial efforts by Western nations to combat the disease, it is estimated that by 2040, more than one-third of the world's population will be affected by cancer [4].

Cancer and other ischemia and inflammatory disorders are characterized by pathological angiogenesis. A growing number of pro- and anti-angiogenic chemicals, some of which are now in clinical trials, have been developed because of concentrated efforts in this sector. The complicated interactions between these molecules, as well as how they influence vascular structure and function in various contexts,

*Address correspondence to this author at the Department of Pharmaceutical Technology, Faculty of Pharmacy, Anadolu University, Eskişehir, Türkiye; E-mail: aaozturk@anadolu.edu.tr

 © 2023 Bentham Science Publishers

have been currently unraveled. This integrated knowledge is resulting in the advancement of a variety of novel and exciting approaches to the treatment of cancer and other diseases [5-7].

Angiogenesis is a natural and complex mechanism that is regulated by biomolecules formed by the body. Endogenous local or systemic chemical signals coordinate endothelial and smooth muscle cell activities to rebuild weakened blood vessels. New blood vessels are formed from pre-existing blood cells by the "sprouting" of endothelial cells, thereby widening the vascular tree. Protease development, endothelial cell migration and proliferation, vascular tube forming, anastomosis of newly formed channels, synthesis of a new basement membrane, and integration of pericytes and smooth muscle cells are all steps toward angiogenesis [8, 9]. Tumor tissue requires oxygen and nutrients to expand or locally metastasize, which would be supplied by blood vessels, and the primary role of blood vessels is to contain oxygen. The availability and concentration of oxygen correlate with endothelial cell metabolism, in which oxygen can be absorbed to form sprouts *in vitro* or a vascular network *in vivo* [10, 11]. There are anti-angiogenesis agents used in cancer treatment, such as axitinib, bevacizumab, cabozantinib, everolimus, lenalidomide, pazopanib, ramucirumab, regorafenib, sorafenib, sunitinib, temsirolimus, thalidomide, vandetanib, and ziv-aflibercept, approved by the FDA [9]. The anti-angiogenesis approach in cancer treatment maintains its popularity today, and many studies have been and continue to be conducted on this subject in the current literature [12-18]. Oxidative stress is closely linked to angiogenesis. Its positive feedback system relies heavily on oxidative damage. The imbalance of the internal oxidation and antioxidant systems, which is linked to the origin and prognosis of many vascular disorders and can be exploited as a biomarker for these disorders, is known as oxidative stress. At the same time, proper oxidative stress management can aid angiogenesis and tissue healing [19-21].

Cancer treatment and diagnosis using nanomedicines are still in the early stages of growth. Compared to traditional chemotherapies, nanotechnology in medicine involves the use of specifically engineered materials for the development of new therapies and devices that minimize toxicity and maximize efficiency in the selective targeting of drugs inside tumor tissue. Abraxane and Doxil are the first nanotechnology-based products that have been approved by the United States Food and Drug Administration (FDA) and are now in the market [22]. Polymer-based nanoparticles, also known as polymeric nanoparticles (NPs), are colloidal structures composed of natural or synthetic polymers. They have major advantages over other nanocarriers, such as liposomes, micelles, and inorganic nanosystems, including the ability to scale up and the production process in accordance with Good Manufacturing Practices (GMP) [23]. Other important properties of polymeric NPs include the widespread availability of different polymers, functionalizing their surface and modulating polymer degradation, and releasing entrapped compounds in response to certain stimuli [23-26].

Poly (lactic-co-glycolic acid) (PLGA) is one of the most well-known biodegradable polymers, with well-defined and adaptable production methods [27]. PLGA is made up of different polymerization ratios of lactic and glycolic acids, which govern its crystallinity and biodegradability under physiological conditions [28]. Due to its specific properties and biocompatibility, the FDA and the European Medicine Agency (EMA) have approved PLGA for use in humans in a variety of drug delivery systems and medical devices [29]. Today, PLGA-based drug delivery systems are a very important field of study [30-34].

Chitosan (CS) is a naturally occurring linear amino polysaccharide that has the ability to enhance the penetration of large molecules through mucosal surfaces while being nontoxic and nonimmunogenic [35]. CS is also recognized as "Generally Recognized as Safe (GRAS)" by the FDA [36]. CS has anticancer, antioxidant, immune enhancing, analgesic, antibacterial, antifungal, wound healing, mucoadhesive, and hemostatic effects. CS can be used to make hydrogels, membranes, beads, porous foams, NPs, *in situ* gel, microparticles, sponges, and nanofibers/scaffolds, either alone or in combination. [37, 38]. CS is commonly used for surface modification in drug delivery systems prepared with various polymers, in addition to being used as a drug delivery polymer in several studies [39-42].

Medicinal inorganic chemistry is rising in popularity and importance because metal-based compounds offer significant chances and possibilities for building novel anti-cancer medicines with promising anti-angiogenic effects [43, 44]. The platinum (Pt) and palladium (Pd) complexes based on metals seem to have promising anticancer properties [45]. Metal complexes have been widely investigated due to their biological activities, especially in the pharmacology area. The anticancer activities of metal complexes have been proven in several studies, and there are even those metal complexes that are available with drug approval, such as cisplatin. Pd complexes are also widely investigated because of their platinum-like chemical and biological characteristics [46, 47]. Today, although almost every research team synthesizes new anticancer substances every day, they remain in the synthesis stage because the relevant active substances cannot be integrated into drug delivery systems.

In this study, we report the successful synthesis and characterization of palladium (II)-carboxamide complex [API code: 950 / $Pd(PyCrbx)_2Cl_2$]. Pyridine carboxamide ligand [API code: 390 / PyCrbx] and its palladium (II) complex have been characterized mainly by single crystal X-ray diffraction analysis and other spectroscopic techniques. To the best of our knowledge, the present study is the first study on the angiogenic evaluation of the copper (II) complex and its free ligands. In this study, 390 and 950 loaded PLGA NPs and chitosan-coated PLGA NPs were formulated and characterized in terms of particle size, polydispersity index, zeta potential, and encapsulation efficiency. In the next stage, after determining whether the formulations were effective in oxidative stress by DPPH analysis, safety tests were carried out on probiotic microorganisms named *Lactobacillus reuterii* DSM 17938 and *Lactobacillus fermentum* CECT 5716. At the last stage, anti-angiogenesis profiles of NPs were determined by *in vivo* Chick Embryo Chorioallantoic Membrane (CAM) assay. When the results were examined, it was found that nanoscale drug carrier systems were prepared, and high antioxidant activity and anti-angiogenesis activity were

detected, especially in NPs prepared with 950. As per our knowledge, this is the first study in this field that will bring a new perspective to cancer treatment.

2. MATERIALS AND METHODS

2.1. Materials

Resomer RG 502 H [*Poly(D, L-lactide-co-glycolide), PLGA, acid terminated, lactide: glycolide 50:50, M_w 7,000-17,000*], acetic acid, and Span 60 [*Sorbitane monostearate*] were purchased from Aldrich Chemical Co. (St. Louis, MO, USA). Low M_w chitosan [*CS, Deacetylated chitin/Poly (d-glucosamine), Mw: 50.000-190.000 Da, viscosity: 20-300 cP*] was purchased from Sigma (Steinheim, Germany). Poloxamer 188 [*a non-ionic surfactant, Poly (ethylene glycol)-block-poly (propylene glycol)-block-poly (ethylene glycol)*] was kindly supplied by BASF (Ataşehir/Istanbul/Turkey). Acetone and Dimethyl sulfoxide (*DMSO*) were purchased from Merck (Darmstadt/Germany). Crystallographic data of palladium (II) complex was collected with Bruker APEX-II CCD using Mo-Ka radiation at room temperature. Nuclear Magnetic Resonance spectra were recorded on a Bruker 400 MHz spectrometer. FT-IR spectra were recorded with Jasco FT/IR-300 E Spectrophotometer using KBr pellets between 4000 and 400 cm^{-1}. Agarose and Sodium Dodecyl Sulfate (*SDS*) were purchased from Fluka (Spain) and Fluka-Biochemika (Germany), respectively. Chloramphenicol, 2,2 Diphenyl 1 picrylhydrazyl (*DPPH*), and (±)-Thalidomide were purchased from Sigma-Aldrich (Germany). The fertilized eggs used in the CAM assay were obtained from Has Tavuk Company (Bursa and Sivrihisar, Turkey). *Lactobacillus reuteri* DSM 17938 and *Lactobacillus fermentum* CECT 5716 were purchased from the commercial Christian Hansen© culture collection. All other chemicals and reagents used were of pharmaceutical and analytical grade.

2.2. Design of APIs

2.2.1. Synthesis of 2-methyl-N-(3-methylpyridine-2-yl) benzamide, [390 / PyCrbx]

Ligand was synthesized in a single step, and the synthesis procedure is depicted in Fig. (**1**). *O*-toluoyl chloride (1 eq, 0.92 mmol) was added drop by drop at a constant temperature to the mixture of 2-amino-3-methylpyridine (1 eq, 0.92 mmol) and triethylamine (NEt_3) (1 eq, 0.92 mmol) in 20 mL THF at 0°C. The resulting mixture was left to stir overnight. After completion of the reaction indicated by TLC, it was filtered, the solvent was evaporated to 5 mL, and the residue was subjected to column chromatography using ethyl acetate:hexane (1:9) solvent mixture. The desired product was obtained as a white crystalline solid. (Yield= 54%), Anal. Calcd (%) for $C_{14}H_{14}N_2O$: C=74.31; H=6.24; N=12.38; Found.: C=74.59; H=6.20; N=12.45. FT-IR (KBr, cm^{-1}): 3212, 2976, 1675, 1581, 1508, 1448, 1287, 1120, 908, 749. ^{1}H-NMR (400 MHz, $CDCl_3$) δ (ppm): 10.33 (s, 1H), 8.25 (s, 1H), 7.68 (s, 1H), 7.46 (s, 1H), 7.34 (s, 1H), 7.24 (d, 3H), 2.40 (s, 3H), 2.24 (s, 3H). ^{13}C-NMR (100 MHz, $CDCl_3$) δ (ppm): 22.01, 22.12, 125.89, 126,12, 131.45, 131.60, 131.95, 132.27, 132.97, 133.62, 141.39, 142.62, 162.96, 172.91.

2.2.2. Synthesis of Palladium (II)/2-methyl-N-(3-methylpyridine-2-yl)benzamide complex, [950 / Pd(PyCrbx)$_2$Cl$_2$]

Palladium complex was synthesized in a single step, and the synthesis procedure is depicted in Fig. (**2**). Ten mL acetonitrile solution of carboxamide ligand (PyCrbx) (127 mg, 0.56 mmol, 2 eq) was added dropwise over 10 minutes to the 10 mL acetonitrile solution of palladium (II) chloride (50 mg, 0.28 mmol, 1 eq) at 60°C, and the resulting solution was left to stir under reflux for 12 hours. After completion of the reaction, it was filtered and left for slow evaporation for over one week. Orange colored X-ray suitable prism crystals were

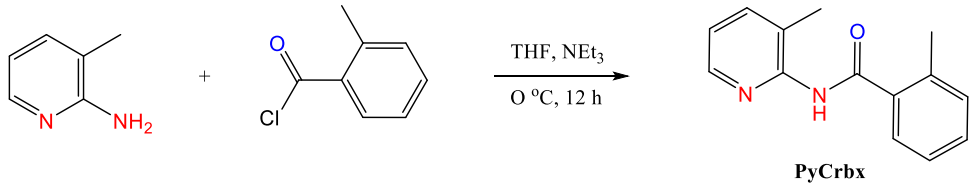

Fig. (1). Ligand (390 / PyCrbx) synthesis procedure. (*A higher resolution / colour version of this figure is available in the electronic copy of the article*).

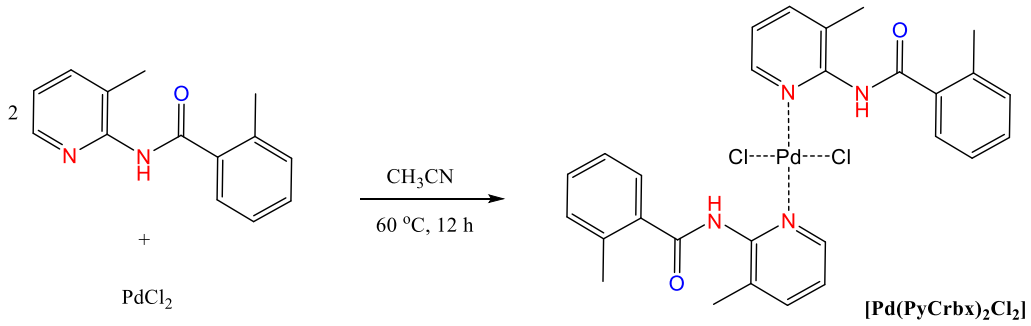

Fig. (2). Palladium complex (950 / [Pd ($PyCrbx)_2Cl_2$]) synthesis procedure. (*A higher resolution / colour version of this figure is available in the electronic copy of the article*).

obtained. (Yield= 67%), Anal. Calcd (%) for $C_{28}H_{28}Cl_2N_4O_2Pd$: C=53.39; H=4.48; N=8.90; Found.: C=53.45; H=4.45; N=8.84. FT-IR (KBr, cm^{-1}): 3219, 2962, 1689, 1444, 1252, 1132, 746, 609.

2.2.3. X-ray Analysis

X-ray data of palladium (II) complex was performed on a Bruker AXS APEX II CCD diffractometer carrying Mo Kα radiation (λ= 0.71073Å) source at 293.15 K and data integration, indexing, and scaling were done by using Bruker SMART program [SMART, Bruker AXS, (2000)] and Olex2 interface. The crystal structure was solved by SHELXT and refined by full-matrix least-squares on all F^2 data using SHELXL [48, 49]. Hydrogen atoms were placed at calculated positions [50]. Molecular structure drawing was performed with the mercury program [51].

2.3. Design of Drug Delivery Systems Loaded with APIs

2.3.1. Preparation of PLGA NPs and Surface Modification with Chitosan

The nanoprecipitation/solvent displacement method, with some modifications, was used to prepare PLGA-based NPs [52-55]. In brief, a weighed amount of PLGA (45 mg) was dissolved in 3 mL of organic solvent mixture (2.5: 0.5, Acetone: DMSO) with Span 60 (15 mg). Next, 3 mL of this solution was added dropwise at a rate of 5 $mL.h^{-1}$ into 10 mL of Poloxamer 188 aqueous solution (0.5%, *w/v*) under magnetic stirring. Acetone was then allowed to evaporate at room temperature under magnetic stirring for 4 h. DMSO was removed by dialysis method [56]. The resulting aqueous dispersion was centrifuged to collect the NPs (11.000 rpm, 45 min, 4°C) (Hettich Rotina-420R, Tuttlingen, Germany). After the NPs were collected, 5 mL of distilled water was added to wash the particles. The NPs dispersed in water were again subjected to the above-mentioned centrifugation process. This process was repeated twice to wash the NPs.

For 390 or 950-loaded PLGA-based NP preparation, briefly, the procedure started by adding 4.5 mg 390 or 950 to the organic phase. Then, 3 mL of such solution with drugs (390 or 950) were added dropwise at a rate of 5 $mL.h^{-1}$ into 10 mL of Poloxamer 188 aqueous solution (0.5%, *w/v*) under magnetic stirring. Acetone was then allowed to evaporate at room temperature under magnetic stirring for 4 h. DMSO was removed by dialysis method [56]. The resulting aqueous dispersion was centrifuged to collect the NPs (11.000 rpm, 45 min, 4°C) (Hettich Rotina-420R, Tuttlingen, Germany). This process was repeated twice to wash the NPs.

When making CS-coated formulations, the above technique was followed with slight changes. In the CS-coated formulations, the aqueous phase consisted of 10 mL of CS solution (0.25%, *w/v*) or 10 mL of Poloxamer 188 aqueous solution (0.5%, *w/v*) or 5 mL of CS solution (0.5%, *w/v*) and Poloxamer 188 aqueous solution (1%, *w/v*). All solutions were prepared with 1% acetic acid (*v/v*) [57-59]. All remaining procedures were the same as above, and the formulation ingredients are presented in Table **1**.

2.4. Characterization of NPs

2.4.1. Particle Size, Polydispersity Index, and Zeta Potential

The particle size (PS), polydispersity index (PDI), and zeta potential (ZP, ζ) of the NPs were determined by dynamic light scattering technique (DLS) on the Zetasizer Nano (Zetasizer Nano ZS, Malvern Instruments, Malvern, UK). The measurements were performed in triplicate at 25 °C after an appropriate dilution (1:10, *v/v*) of the NP suspensions in Milli-Q® water [60].

2.4.2. UV Spectrophotometric Method for Drugs

Prior to the encapsulation efficiency (EE %) study, specific and selective UV spectrophotometric methods were developed for 390 and 950. The UV method was performed on a UV/vis spectrophotometer (UV-160A, Shimadzu, Japan) at 270 nm and 273 nm for 390 and 950, respectively, using a quartz cell. The stock solutions of 390 or 950 were prepared at a concentration of 1000.0 $\mu g.mL^{-1}$. Stock solutions were created using distilled water: DMSO (1:1, v/v). The stock concentration of 20 $\mu g.mL^{-1}$ was measured with a spectrophotometer at 200-800 nm [61]. A series of dilutions consisted of 6 different concentrations of 390 or 950in the range of 1.0-20.0 $\mu g.mL^{-1}$. Absorbance values were measured, and calculations were made to determine 390 and 950 concentrations. The Limit of Detection (LOD) and Limit of Quantitation (LOQ) were separately determined based on the calibration curve obtained according to ICH Q2 (R1) recommendations. Intermediate precision and repeatability values using the device were verified by repeated scanning and measurement of absorbance's for 390 and 950 (5.0 $\mu g.mL^{-1}$, 10.0 $\mu g.mL^{-1}$, 15.0 $\mu g.mL^{-1}$). Repeating tests on three consecutive days verified the intermediate precision of the method. Results were expressed as RSD% of the measurements obtained. The method's accuracy was determined by calculating drug recoveries using the standard addition method. Standard solutions containing a specific amount of 390 or 950 (5.0 $\mu g.mL^{-1}$, 10.0 $\mu g.mL^{-1}$, 15.0 $\mu g.mL^{-1}$) were used, and the percentage of recoveries was calculated [62, 63].

2.4.3. Encapsulation Efficiency (EE %)

The accurately weighed NPs (5 mg) were added to distilled water: DMSO (1: 1), and the probe was sonicated for 1 minute at 60% power, thereby disrupting the nanoparticle structure. The resultant samples were filtered through 0.45 mm membrane filters and analyzed using a UV/visible spectrophotometer (UV-160 Shimadzu) at λ_{max} =270 nm and λ_{max} =273 nm for 390 and 950, respectively. The encapsulation efficiency (EE%) of nanoparticles is calculated by Formula (1) [64, 65].

$$EE\ \% = \left[\frac{Total\ amount\ of\ drug\ added - Amount\ of\ free\ drug}{Total\ amount\ of\ drug\ added}\right] x100 \quad (1)$$

2.5. *In vitro* Antioxidant Activity-free Radical Scavenging Assay (DPPH Test)

The scavenging effect of the samples on DPPH free radical was determined using a modified method of Brand-Williams [66]. The free radical scavenging activity of the

Table 1. Formulation ingredients.

Code	PLGA	Span 60	ACN	DMSO	390	950	P 188-1	CS-1	P-188-2	CS-2
NP-Blank-P	45 mg	15 mg	2.5 mL	0.5 mL	-	-	10 mL	-	-	-
NP-Blank-CSP1	45 mg	15 mg	2.5 mL	0.5 mL	-	-	-	10 mL	-	-
NP-Blank-CSP2	45 mg	15 mg	2.5 mL	0.5 mL	-	-	-	-	5 mL	5 mL
NP-390-P	45 mg	15 mg	2.5 mL	0.5 mL	4.5 mg	-	10 mL	-	-	-
NP-390-CSP1	45 mg	15 mg	2.5 mL	0.5 mL	4.5 mg	-	-	10 mL	-	-
NP-390-CSP2	45 mg	15 mg	2.5 mL	0.5 mL	4.5 mg	-	-	-	5 mL	5 mL
NP-950-P	45 mg	15 mg	2.5 mL	0.5 mL	-	4.5 mg	10 mL	-	-	-
NP-950-CSP1	45 mg	15 mg	2.5 mL	0.5 mL	-	4.5 mg	-	10 mL	-	-
NP-950-CSP2	45 mg	15 mg	2.5 mL	0.5 mL	-	4.5 mg	-	-	5 mL	5 mL

Note: PLGA: Resomer RG 502 H, ACN: Acetone, DMSO: Dimethyl sulfoxide, P-188-1: Poloxamer 188 aqueous solution (0.5%, *w/v*), CS-1: CS solution (0.25%, *w/v*), P-188-2: Poloxamer 188 aqueous solution (1.0%, *w/v*), CS-2: CS solution (0.5%, *w/v).*

samples was expressed as a percentage of inhibition calculated according to Formula (2):

$$Inh\ \% = \left[\frac{A_{control} - A_{sample}}{A_{control}}\right] x100 \quad (2)$$

Where $A_{control}$ is the absorbance of the control (containing all reagents except the test compound), A_{sample} is the absorbance of the sample with added DPPH. The IC_{50} values were obtained by plotting the DPPH scavenging percentage of each sample against the sample concentration. Data were analyzed using the SigmaPlot software (Version 12.0).

2.6. Antimicrobial Activity

2.6.1. Microorganisms and Culture Conditions

Probiotic microorganism strains were purchased from the Christian Hansen© culture collection. The routine culture was performed on MRS Agar (Biokar Diagnostics©, Ref: BK089HA) for *Lactobacillus reuteri* DSM 17938 and *Lactobacillus fermentum* CECT 5716 microorganisms [66, 67]. All agar plates were incubated at 37°C for 24 -36 h. Several colonies of each microorganism were then suspended in % 0.9 NaCl, and cell suspensions were adjusted to c.10^8 CFU mL^{-1} and 0.5 Mc Farland turbidity [68].

2.6.2. Agar Dilution Minimum Inhibitor Concentration (MIC) Method

Bacteria were assessed for susceptibility to 390, 950, and NPs using agar dilution assay, which was performed according to method M7-A7 from the Clinical Laboratory Standards Institute (CLSI) [69, 70]. Chloramphenicol was used as a positive control. A stock solution of 390, 950, and NPs was prepared in sterile distilled water at 200, 400, and 400 $\mu g.mL^{-1}$, Chloramphenicol was dissolved in %10 (*v/v*) respectively. Appropriate volumes of NPs, active ingredients stock solution sterile distilled water, and MRS agar were combined, resulting in final concentrations of 400 $\mu g.mL^{-1}$, 200 $\mu g.mL^{-1}$ and 100 $\mu g.mL^{-1}$ for active ingredients and 100 $\mu g.mL^{-1}$, 50 $\mu g.mL^{-1}$and 25 $\mu g.mL^{-1}$for the NPs. Inocula were prepared as described earlier, and agar plates were inoculated using sterile pipetting sets that delivered a 50 µL inoculum spot, corresponding to c. 10^4 CFU per spot. Plates were incubated for 24 h at 37°C, and minimum inhibitory concentrations (MICs) were then determined as the lowest inhibiting growth concentration [71].

2.7. The *In vivo* Anti-angiogenic Activity

2.7.1. Preparation of Test Samples

In this study, 390 loaded NPs (including PyCrbx as 50 $\mu g.egg^{-1}$), 950 loaded NPs (including $Pd(PyCrbx)_2Cl_2$ as 50 $\mu g.egg^{-1}$), blank formulations (50 $\mu g.egg^{-1}$), 390 (50 $\mu g.egg^{-1}$) and 950 (50 $\mu g.egg^{-1}$) and standards (50 $\mu g.egg^{-1}$) were dissolved/suspended in a 2.5% (*w/v*) agarose solution. For ease of application, pellets of these solutions (10 µL) were prepared and applied dropwise on circular stainless-steel supports of 5 mm diameter and cooled to room temperature for solidification, and then applied to the chick chorioallantoic membrane (CAM).

2.7.2. The In vivo Chick Embryo Chorioallantoic Membrane (CAM) Assay

The *in vivo* CAM assay was performed as described in the previous work reported by our research team [72]. The previously incubated fertilized hen eggs for 72 h at 36.5°C and a relative humidity of 80% were positioned in a horizontal position and rotated several times. The eggs were opened on the snub side, and furthermore, 10-15 mL of albumin were aspirated from them. The eggs were traced with a scalpel at the two third of the height (from the pointed side), and after that, the shells were removed with forceps. The cavity was covered with film, and they were incubated at 36.5°C at a relative humidity of 80% for a further 72 h. Pellets were placed on the CAM, which had approximately a diameter of 2 cm. One day later, the eggs were evaluated under the stereomicroscope. A total of 10-15 eggs were utilized for each test compound. All compounds were tested in triplicate at different times.

Anti-angiogenic effects were evaluated by using a scoring system (Table **2**). The anti-angiogenic scores were calculated using Formula (3) for scoring. Positive control (±)-thalidomide and negative control sodium dodecyl sulphate (SDS) at the concentration of 50 µg.egg^{-1} were also tested. CAMs treated with solidified agarose-solution in pellet form (2.5%, *w/v*) were also tested as a blank. Tests for each compound were performed in triplicate [72].

Table 2. Semi-quantitative score system of anti-angiogenic effect on CAM after treatment.

Scale	Anti-angiogenic Effect	Effects Observed on CAM after Treatment
<0.5	Inactive	No change (Normal embryo growth).
0.5-0.75	Weak	No capillary-free area. Area with reduced density of capillaries around the pellet not larger than its own area.
>0.75-1	Strong	Small capillary-free area or area with significantly reduced density of capillaries. Effects not larger than double the size of the pellet.
>1	Very strong	Capillary free area around the pellet at least doubles the size of the pellet.

$$Average\ score = \frac{Number\ of\ eggs\ (score\ 2)\times 2 + number\ of\ eggs\ (score\ 1)\times 1}{total\ number\ of\ eggs\ (score\ 0,1,2)} \quad (3)$$

2.8. Statistical and Mathematical Analysis

Microsoft Excel was employed for mathematical analysis. All data obtained were evaluated statistically (one-way ANOVA test) using GraphPad Prism version 7.0. All measurements were done for at least three replicates. In all studies, $p < 0.05$ was of statistical significance. The results were each presented as Mean ± SD.

3. RESULTS AND DISCUSSION

3.1. Synthesis and Characterization of APIs

Carboxamide ligand (API code: 390, PyCrbx) was obtained by the reaction between 2-amino-3-methylpyridine and o-toluoyl chloride under basic conditions in high yields. Palladium(II) complex (API code: 950, $[Pd(PyCrbx)_2Cl_2]$) was synthesized by the reaction of a respective ligand with palladium(II) chloride in refluxing acetonitrile medium.

3.1.1. X-ray Structure Analysis of [Pd (PyCrbx)$_2$Cl$_2$] Complex

The coordination reaction of PyCrbx (390) ligand and palladium (II) chloride salt resulted in the title $[Pd(PyCrbx)_2Cl_2]$ (950) complex. The crystal data of the palladium (II) complex was obtained from a light orange rectangular prism crystal. The thermal ellipsoid structure of the palladium (II) complex is given in Fig. (**3**). Crystallographic data, bond distances, and angles are given in Tables **3** and **4**.

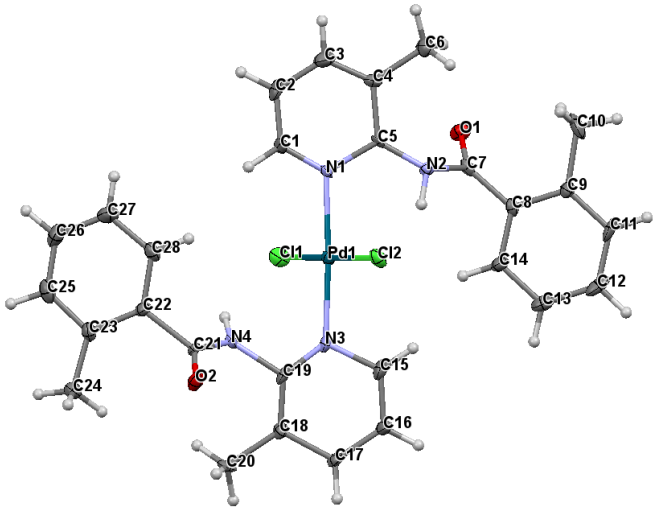

Fig. (3). Thermal ellipsoid plots of the Palladium(II)/2-methyl-N-(3-methylpyridine-2-yl)benzamide, ($[Pd(PyCrbx)_2Cl_2]$) complex at the 40% probability level. (*A higher resolution / colour version of this figure is available in the electronic copy of the article*).

From the crystallographic data, the mononuclear palladium (II) complex shows a triclinic *P*1 space group. In the crystal structure of the palladium (II) complex, the metal center is surrounded by two carboxamide ligands and two chlorine anions by *trans*- positions. The palladium (II) center adopted slightly distorted square-planar geometry with average values for Pd-N distance was 2.0459 Å and average Pd-Cl distance was 2.2939 Å, which were in agreement with those reported in analogous complexes [73-75]. The dihedral angle between the pyridine part of the ligand and the chlorine atom was calculated as 62.94º. Pyridine rings and phenyl rings of two identical ligands were found to be parallel to each other. The square planar geometry around Pd(II) center coordination angles measured between 87.345º and 92.743º.

3.2. Preparation of PLGA Nanoparticles and Surface Modification with Chitosan

3.2.1. Particle Size, Polydispersity Index, Zeta Potential

Characterizations of NPs are primarily evaluated with PS, PDI, and ZP. The relevant information is presented in Table **5**. PS obtained in the blank formulation was 82.4-473.9 nm, while PS in the API-loaded NPs was 193.2-678.0 nm. In PS analysis, it is important to note that PS increases with API loading. This situation is supported by the literature [76]. PS of NPs prepared with CS increased about twofold compared to those prepared with PLGA alone. This may be explained due to CS-related viscosity increase, which reduces the shear stress during the emulsion mixing on the magnetic stirrer and then leads to an increase in the PS of emulsion droplets [54]. Formulations prepared with a surfactant (Poloxamer 188) added to the CS solution were found to have smaller PSs. The presence of a surfactant in the aque-

ous phase during preparation reduces the surface tension and stabilizes newly developed surfaces during nanoprecipitation and the production of smaller particles [77].

Table 3. Crystal data and structure refinement for [Pd(PyCrbx)$_2$Cl$_2$] complex (API code: 950).

Empirical Formula	$C_{28}H_{28}N_4O_2Cl_2Pd$
Formula weight	629.84
Temperature	293.15 K
Wavelength	0.71073 Å
Crystal system, space group	Triclinic, *P*1
Unit cell dimensions	a = 6.7157(4) Å alpha =87.352(2) ° b = 8.0671(5) Å beta = 77.821(2) ° c = 14.1650(8) Å gamma = 66.124(2) °
Volume	685.28(7) A^3
Z, Calculated density	1, 1.526 Mg/m^3
Absorption coefficient	0.905 mm^{-1}
F(000)	320.0
Crystal size	0.2 x 0.1 x 0.1 mm
Theta range for data collection	5.89 to 56.734 deg
Limiting indices	-8<=h<=8, -10<=k<=10, -18<=l<=18
Reflections collected / unique	22135/6787 [R(int) = 0.0398]
Completeness to theta	28.367 99 %
Absorption correction	Integration
Refinement method	Full-matrix least-squares on F^2
Data/restraints/parameters	6787 / 3 / 326
Goodness-of-fit on F^2	1.033
Final R indices [I>2sigma(I)]	R1 = 0.0347, wR2 = 0.0706
R indices (all data)	R1 = 0.0477, wR2 = 0.0752
Largest diff. peak and hole	0.36 and -0.57 $e.A^{-3}$

Table 4. Selected bond distances (Å) and bond angles (°).

Bond Distances (Å)	Bond Angles (°)
Pd(1)-N(1) 2.0565(10)	N(1)-Pd(1)-Cl(1) 87.345(3)
Pd(1)-N(3) 2.0354(10)	Cl(1)-Pd(1)-N(3) 88.854(3)
Pd(1)-Cl(1) 2.2914(14)	N(3)-Pd(1)-Cl(2) 91.072(3)
Pd(1)-Cl(2) 2.2965(14)	Cl(2)-Pd(1)-N(1) 92.743(3)

It was observed that the PDI values increased proportionally with an increase in PS. PDI value, which defines particle size distribution, was reported to be in the range of 0.01 and 0.7 for monophasic systems; a value higher than 0.7 is indicative of a very wide PS distribution, and a value close to zero means narrow PS distribution [78]. According to this literature, it can be observed that the modified nanoparticles move away from monodispersity, especially with Poloxamer 188 unused chitosan solution.

The ZP of formulations is presented in Table **5**. If the ZP has a high positive or negative value in colloidal systems, the particles repel each other. A colloidal system having ± 30 mV as the ZP value is considered a stable formulation if dispersed as a colloidal dispersion in a liquid [79]. The ZP values between −5.0 and −15.0 mV were in the limited flocculation zone, and the maximum flocculation zone between −5.0 and −3.0 mV was reported earlier [80]. When all the results were examined, it was found that ZP values were at the limit of flocculation. This shows the relative stability of all formulations prepared.

As shown in Table **5**, negative ZP values are observed in uncoated PLGA NPs. PLGA in a neutral medium has negative surface potential, attributed to the terminal carboxyl groups, and this could be verified by the ZP of negative obtained in uncoated PLGA NPs [57]. In surface-modified formulations with CS, the ZP of the NPs increased significantly to positive values. This is a consequence of the amino groups present in this polysaccharide, suggesting that the PLGA NPs were adequately coated by CS [57]. Besides the high stability promoted by this high ZP value, positive surface charges are attracted by the negatively charged cell membranes, promoting adhesion and retention of the system at the site of action and in the intestinal epithelium, as well as increasing the absorption of the nanometric system [81]. In addition, the presence of CS may decrease the absorption and interaction of NPs by phagocytes because this absorption occurs more frequently on hydrophobic and negatively charged surfaces [82].

As a result, when all PS, ZP, and PDI values were evaluated, appropriate results were obtained in terms of drug use.

3.2.2. UV Spectrophotometric Method

Following validation of the UV-Visible spectrophotometric method developed for 390, linearity was determined to be at a concentration range of 1.0-15.0 $\mu g.mL^{-1}$ (1.0 $\mu g.mL^{-1}$, 2.5 $\mu g.mL^{-1}$, 5.0 $\mu g.mL^{-1}$, 7.5 $\mu g.mL^{-1}$, 10.0 $\mu g.mL^{-1}$, 15.0 $\mu g.mL^{-1}$) with linearity of y = 0.0398x-0.0137 (r^2 = 0.9997). This method was found to be precise due to relative standard deviation (RSD) values of < 2% for repeatability and intermediate precision. Recovery and accuracy of the method were satisfactory owing to < 2% RSD value. Accuracy values of 99.171 ± 1.535% (Mean ± SD), 100.259 ± 0.145% (Mean ± SD), and 99.338 ± 0.953% (Mean ± SD) for concentrations of 5.0, 10.0, and 15.0 $\mu g.mL^{-1}$, respectively, were determined for the UV-Visible spectrophotometric method. The limit of detection (LOD) was determined to be 0.225 $\mu g.mL^{-1}$ while the limit of quantitation (LOQ) was 0.683 $\mu g.mL^{-1}$. In the selectivity study, blank formulations were photometrically examined between 200 and 800 nm and did not yield any absorbance peak at 270 nm in distilled water: DMSO (1:1, v/v).

Following validation of the UV-Visible spectrophotometric method developed for 950, linearity was determined to be

Table 5. Particle size, polydispersity index, and zeta potential and encapsulation efficiency.

Code	PS	PDI	ZP	EE %
NP-Blank-P	82.403 ± 0.992	0.189 ± 0.009	-14.869 ± 1.804	-
NP-Blank-CSP1	473.900 ± 18.720	0.540 ± 0.044	29.800 ± 3.874	-
NP-Blank-CSP2	342.633 ± 2.113	0.275 ± 0.019	30. 267 ± 1.950	-
NP-390-P	193.267 ± 2.970	0.171 ± 0.059	-14.633 ± 1.804	79.023 ± 1.036
NP-390-CSP1	600.800 ± 34.760	0.797 ± 0.137	32.167 ± 1.258	68.018 ± 0.084
NP-390-CSP2	361.967 ± 5.823	0.197 ± 0.031	30.200 ± 2.821	67.695 ± 1.164
NP-950-P	262.067 ± 6.586	0.227 ± 0.043	-13.450 ± 0.651	61.364 ± 0.965
NP-950-CSP1	678.033 ± 96.838	0.837 ± 0.042	31.133 ± 1.159	53.154 ± 1.897
NP-950-CSP2	441.133 ± 5.701	0.361 ± 0.032	31.633 ± 1.450	55.062 ± 0.366

at a concentration range of 2.5-20 $\mu g.mL^{-1}$ (2.5 $\mu g.mL^{-1}$, 5.0 $\mu g.mL^{-1}$, 7.5 $\mu g.mL^{-1}$, 10.0 $\mu g.mL^{-1}$, 15.0 $\mu g.mL^{-1}$, 20.0 $\mu g.mL^{-1}$) with linearity of y = 0.0039x-0.0069 (r^2 = 0.9998). This method was reported to be precise due to relative standard deviation (RSD) values of < 2% for repeatability and intermediate precision. Recovery and accuracy of the method were satisfactory owing to < 2% RSD value. Accuracy values of 99.762 ± 1.467% (Mean ± SD), 100.190 ± 0.763% (Mean ± SD), and 100.568 ± 1.051% (Mean ± SD) for concentrations of 5.0, 10.0, and 15.0 $\mu g.mL^{-1}$, respectively, were determined for the UV-Visible spectrophotometric method. The limit of detection (LOD) was determined to be 0.264 $\mu g.mL^{-1}$ while the limit of quantitation (LOQ) was 0.800 $\mu g.mL^{-1}$. In the selectivity study, blank formulations were photometrically examined between 200 and 800 nm and did not yield any absorbance peak at 273 nm in distilled water: DMSO (1:1, v/v). Consequently, the easy and inexpensive procedures proposed in this study can be used for routine and simultaneous 390 and 950 coded drug determination [83-86].

3.2.3. Encapsulation Efficiency

Drug EE of NPs is an important factor in formulations because higher loading leads to a lower number of NPs for a given dose of treatment [87]. The high values of encapsulation for PLGA NPs achieved were probably due to the lipophilic nature of the API, presenting low affinity to water phases and thus tending to migrate to the organic phase [58]. A decrease in EE% was observed in CS-coated PLGA NPs compared to uncoated PLGA NPs. When the cause of this condition was investigated in the literature, similar results were obtained in CS-coated paclitaxel-loaded PLGA NPs. This can be explained briefly as a possible cause of CS hydrophilicity, which may prevent the entrapment of hydrophobic drugs [88]. As a result, EE results were obtained in terms of drug administration in all NPs.

3.3. *In vitro* Antioxidant Activity-free Radical Scavenging Assay (DPPH Test)

As *in vitro* antioxidant activity of 950, 390, and NPs was evaluated by using the DPPH scavenging method, among the formulations, NP-950-P showed the highest antioxidant activity with IC_{50} = 3.025 $\mu g.mL^{-1}$ whereas NP-950-CSP2 showed the lowest antioxidant potential (IC_{50} = 34.61 $\mu g.mL^{-1}$) when compared with Vit C (IC_{50} = 1.6522 $\mu g.mL^{-1}$).

Among the formulations, NP-950-P, NP-390-P, and NP-350-CSP2 were found to have significant antioxidant potentials with IC_{50} values of 3.025, 5.198, and 7.4242 $\mu g.mL^{-1}$, respectively, when compared to Vit C, as shown in Fig. (**4**).

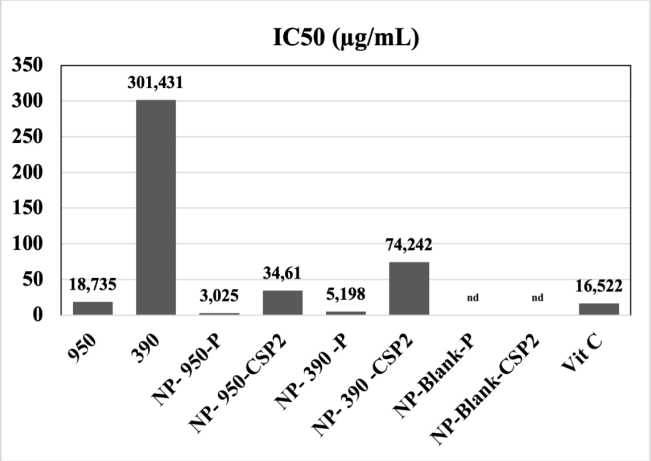

Fig. (4). *In vitro* antioxidant-DPPH scavenging activity of samples. **Abbreviation: *nd**: no activity detected.

3.4. Antimicrobial Activity Results

The *in vitro* antimicrobial activity results against the probiotics *L. reuteri* and *L. fermentum* showed that NP-950-CSP2 and NP-390-CSP2 significantly inhibited the facultative anaerobic *L. reuteri* bacteria at 200 and 100 $\mu g.mL^{-1,}$ respectively, when compared with chloramphenicol. The antimicrobial effectiveness of the other samples was not significant against *L. reuteri* and *L. fermentum*. Moreover, these results indicated that the formulations were safe against tested gram-positive facultative anaerobic microorganisms (Table **6**).

Table 6. Antimicrobial activity results.

Sample	Microorganisms/MICs (µg/mL)	
-	*L. reuteri*	*L. fermentum*
950 ($Pd(PyCrbx)_2Cl_2$)	>400	>400
390 (PyCrbx)	>400	>400
NP- 950-P	>400	>400
NP- 950-CSP2	>400	200
NP- 390 -P	400	>400
NP- 390 -CSP2	400	>100
NP-Blank-P	nd	nd
NP-Blank-CSP2	nd	nd
Chloramphenicol	<25	<25

Abbreviation: *nd: no activity detected.

3.5. *In vivo* Anti-angiogenic Effects

The anti-angiogenic activities of 390, 950, and NPs were examined using the CAM assay. (±)-Thalidomide was used as a positive control, whereas sodium dodecyl sulphate was employed as a negative control for the assay. The results are summarized in Table **7**. For the evaluation of anti-angiogenic effect, a semi-quantitative score system was used, as shown in Table **2** [72].

According to the microscopic evaluations (Fig. **5**), NP-950-P (including $Pd(PyCrbx)_2Cl_2$ as 50 µg.egg^{-1}) and NP-950-CSP2 (including $Pd(PyCrbx)_2Cl_2$ as 50 µg.egg^{-1}) showed strong anti-angiogenic effect with the scores of 0.9 ± 0.2 and 0.76 ± 0.14, respectively whereas the other NP formulations showed a weak anti-angiogenic effect when compared with the positive control (±)-Thalidomide with the score of (0.85 ± 0.3) at the concentration of 50 µg.egg^{-1}. An important observation resulting in the interaction of the test samples was NP-Blank-CSP2, which showed significant membrane irrita-

Table 7. Anti-angiogenic effects of 950, 390, and NPs using the *in vivo* CAM-assay.

Sample	Concentration (*µ*g.pellet^{-1})	Average Score[a]	Anti-angiogenic Effect	Irritation/Tox (%)
950 ($Pd(PyCrbx)_2Cl_2$)	50	0.7 ± 0.1	Weak	-
390 (PyCrbx)	50	0.6 ± 0.1	Weak	-
NP- 950-P	including $Pd(PyCrbx)_2Cl_2$ as 50	0.9 ± 0.2	Strong	-
NP- 950-CSP2	including $Pd(PyCrbx)_2Cl_2$ as 50	0.76 ± 0.14	Strong	25.20 ± 5
NP- 390 -P	including PyCrbx as 50	0.7 ± 0.08	Weak	-
NP- 390 -CSP2	including PyCrbx as 50	0.6 ± 0.06	Weak	-
NP-Blank-P	50	0.5 ± 0.2	Inactive	-
NP-Blank-CSP2	50	0.4 ± 0.1	Inactive	60.05 ± 4
Agarose (Blank)	%2.5, w/v	0.4 ± 0.1	Inactive	-
(±)-Thalidomide (Positive control)	50	0.85 ± 0.3	Strong	-
Sodium dodecyl sulfate (SDS) (Negative control)	50	0.1 ± 0.1	Inactive	84 ± 2

Note: [a] Values are mean of average score ± Standard deviation (n = 45 for the test substances and n = 30 for standards). **p* < 0.05 compared with (±)-Thalidomide.

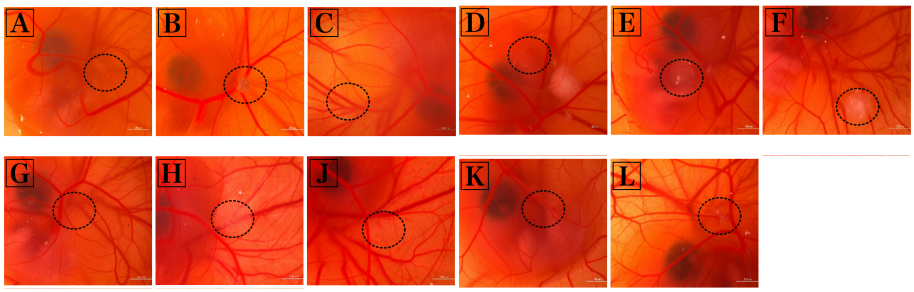

Fig. (5). *In vivo* CAM-assay results: (**A**) CAM treated with (±)-Thalidomide; (**B**) Membrane irritation with SDS; (**C**) Normal embryo growth with Agarose; (**D**) Strong anti-angiogenic effect of NP- 950-P; (**E**) Strong anti-angiogenic effect of NP- 950-CSP2 with slight irritation; (**F**) Weak anti-angiogenic effect of NP- 390 -P; (**G**) Weak anti-angiogenic effect of NP- 390 -CSP2; (**H**) Weak anti-angiogenic effect of 950 ($Pd(PyCrbx)_2Cl_2$); (**J**) Weak anti-angiogenic effect of 390 (PyCrbx); (**K**) No anti-angiogenic effect of NP-Blank-P; (**L**) No anti-angiogenic effect of NP-Blank-CSP2 with significant membrane irritation. (*A higher resolution / colour version of this figure is available in the electronic copy of the article*).

tion, and NP-950-CSP2 showed slight membrane irritation, whereas the other samples also showed neither membrane irritation nor toxicity at the tested concentration.

CONCLUSION

When the results obtained were examined, it was found that nanoscale drug carrier systems were prepared, and high antioxidant activity and anti-angiogenesis activity were detected, especially in nanoparticles prepared with 950. As per our knowledge, this is the first study conducted in this field, which will bring a new perspective to cancer treatment.

LIST OF ABBREVIATIONS

CAM	=	Chorioallantoic Membrane
CS	=	Chitosan
EMA	=	Medicine Agency
FDA	=	Food and Drug Administration
GMP	=	Good Manufacturing Practices
LOD	=	Limit of Detection
LOQ	=	Limit of Quantitation
NPs	=	Polymeric Nanoparticles
PLGA	=	Poly Lactic-co-glycolic Acid
RSD	=	Relative Standard Deviation
SDS	=	Sodium Dodecyl Sulfate
WHO	=	World Health Organization

ETHICS APPROVAL AND CONSENT TO PARTICIPATE

Not applicable.

HUMAN AND ANIMAL RIGHTS

No animals/humans were used for studies that are the basis of this research.

CONSENT FOR PUBLICATION

Not applicable.

AVAILABILITY OF DATA AND MATERIALS

The data and supportive information are available within the article.

FUNDING

This study was financed by Anadolu University Scientific Research Project Foundation (Grant no: 2005S059).

CONFLICT OF INTEREST

The authors declare no conflict of interest, financial or otherwise.

ACKNOWLEDGEMENTS

The authors would like to thank Mrs. Emine Kırcalı Kocabaş from Has Tavuk Company for providing the fertilized hen eggs. They would also like to thank Alper Çimik and Tuğba Nur Tüysüz for helping during the experimental phase.

SUPPLEMENTARY MATERIAL

Supplementary material is available on the publisher's website along with the published article.

REFERENCES

[1] İlem-Özdemir, D.; Karavana, S.Y.; Şenyiğit, Z.A.; Çalışkan, Ç.; Ekinci, M.; Asikoglu, M.; Baloğlu, E. Radiolabeling and cell incorporation studies of gemcitabine HCl microspheres on bladder cancer and papilloma cell line. *J. Radioanal. Nucl. Chem.,* **2016**, *310*(2), 515-522. http://dx.doi.org/10.1007/s10967-016-4805-6

[2] Ekinci, M.; İlem-Özdemir, D. Nanoteranostikler. *Ankara Univers. Eczacilik Fakult. Dergisi,* **2021**, *45*, 131-155. http://dx.doi.org/10.33483/jfpau.717067

[3] Sedrak, M.S.; Freedman, R.A.; Cohen, H.J.; Muss, H.B.; Jatoi, A.; Klepin, H.D.; Wildes, T.M.; Le-Rademacher, J.G.; Kimmick, G.G.; Tew, W.P.; George, K.; Padam, S.; Liu, J.; Wong, A.R.; Lynch, A.; Djulbegovic, B.; Mohile, S.G.; Dale, W. Older adult participation in cancer clinical trials: A systematic review of barriers and interventions. *CA Cancer J. Clin.,* **2021**, *71*(1), 78-92. http://dx.doi.org/10.3322/caac.21638 PMID: 33002206

[4] Casado, J. Proteogenomics methods for translational cancer research. Doctoral Dissertation. Research Program in Systems Oncology. University of Helsinki, Finland, April **2021**.

[5] Carmeliet, P.; Jain, R.K. Angiogenesis in cancer and other diseases. *Nature,* **2000**, *407*(6801), 249-257. http://dx.doi.org/10.1038/35025220 PMID: 11001068

[6] Nishida, N.; Yano, H.; Nishida, T.; Kamura, T.; Kojiro, M. Angiogenesis in cancer. *Vasc. Health Risk Manag.,* **2006**, *2*(3), 213-219. http://dx.doi.org/10.2147/vhrm.2006.2.3.213 PMID: 17326328

[7] Yang, Y.; Sun, M.; Wang, L.; Jiao, B. HIFs, angiogenesis, and cancer. *J. Cell. Biochem.,* **2013**, *114*(5), 967-974. http://dx.doi.org/10.1002/jcb.24438 PMID: 23225225

[8] Carmeliet, P. Mechanisms of angiogenesis and arteriogenesis. *Nat. Med.,* **2000**, *6*(4), 389-395. http://dx.doi.org/10.1038/74651 PMID: 10742145

[9] Rajabi, M.; Mousa, S. The role of angiogenesis in cancer treatment. *Biomedicines,* **2017**, *5*(4), 34. http://dx.doi.org/10.3390/biomedicines5020034 PMID: 28635679

[10] Helmlinger, G.; Endo, M.; Ferrara, N.; Hlatky, L.; Jain, R.K. Formation of endothelial cell networks. *Nature,* **2000**, *405*(6783), 139-141. http://dx.doi.org/10.1038/35012132 PMID: 10821260

[11] Hansen-Algenstaedt, N.; Stoll, B.R.; Padera, T.P.; Dolmans, D.E.; Hicklin, D.J.; Fukumura, D.; Jain, R.K. Tumor oxygenation in hormone-dependent tumors during vascular endothelial growth factor receptor-2 blockade, hormone ablation, and chemotherapy. *Cancer Res.,* **2000**, *60*(16), 4556-4560. PMID: 10969807

[12] Zhu, S.; Ye, L.; Bennett, S.; Xu, H.; He, D.; Xu, J. Molecular structure, gene expression and functional role of WFDC1 in angiogenesis and cancer. *Cell Biochem. Funct.,* **2021**, *39*(5), 588-595. http://dx.doi.org/10.1002/cbf.3624 PMID: 33615507

[13] Bai, J.Y.; Jin, B.; Ma, J.B.; Liu, T.J.; Yang, C.; Chong, Y.; Wang, X.; He, D.; Guo, P. HOTAIR and androgen receptor synergistically increase GLI2 transcription to promote tumor angiogenesis and cancer stemness in renal cell carcinoma. *Cancer Lett.,* **2021**, *498*, 70-79. http://dx.doi.org/10.1016/j.canlet.2020.10.031 PMID: 33157157

[14] Yousefi, H.; Vatanmakanian, M.; Mahdiannasser, M.; Mashouri, L.; Alahari, N.V.; Monjezi, M.R.; Ilbeigi, S.; Alahari, S.K. Understanding the role of integrins in breast cancer invasion, metastasis,

angiogenesis, and drug resistance. *Oncogene,* **2021**, *40*(6), 1043-1063.
http://dx.doi.org/10.1038/s41388-020-01588-2 PMID: 33420366

[15] Zhou, L.; Yin, R.; Gao, N.; Sun, H.; Chen, D.; Cai, Y.; Ren, L.; Yang, L.; Zuo, Z.; Zhang, H.; Zhao, J. Oligosaccharides from fucosylated glycosaminoglycan prevent breast cancer metastasis in mice by inhibiting heparanase activity and angiogenesis. *Pharmacol. Res.,* **2021**, *166*, 105527.
http://dx.doi.org/10.1016/j.phrs.2021.105527 PMID: 33667689

[16] Yin, H.; Yu, S.; Xie, Y.; Dai, X.; Dong, M.; Sheng, C.; Hu, J. Cancer-associated fibroblasts-derived exosomes upregulate microRNA-135b-5p to promote colorectal cancer cell growth and angiogenesis by inhibiting thioredoxin-interacting protein. *Cell. Signal.,* **2021**, *84*, 110029.
http://dx.doi.org/10.1016/j.cellsig.2021.110029 PMID: 33932496

[17] Xue, R.; Sheng, Y.; Duan, X.; Yang, Y.; Ma, S.; Xu, J.; Wei, N.; Shang, X.; Li, F.; Wan, J.; Qin, Z. Tie2-expressing monocytes as a novel angiogenesis-related cellular biomarker for non-small cell lung cancer. *Int. J. Cancer,* **2021**, *148*(6), 1519-1528.
http://dx.doi.org/10.1002/ijc.33381 PMID: 33152113

[18] Leng, Y.; Chen, Z.; Ding, H.; Zhao, X.; Qin, L.; Pan, Y. Overexpression of microRNA-29b inhibits epithelial-mesenchymal transition and angiogenesis of colorectal cancer through the ETV4/ERK/EGFR axis. *Cancer Cell Int.,* **2021**, *21*(1), 17.
http://dx.doi.org/10.1186/s12935-020-01700-2 PMID: 33407520

[19] Huang, Y.J.; Nan, G.X. Oxidative stress-induced angiogenesis. *J. Clin. Neurosci.,* **2019**, *63*, 13-16.
http://dx.doi.org/10.1016/j.jocn.2019.02.019 PMID: 30837109

[20] Tertil, M.; Jozkowicz, A.; Dulak, J. Oxidative stress in tumor angiogenesis-therapeutic targets. *Curr. Pharm. Des.,* **2010**, *16*(35), 3877-3894.
http://dx.doi.org/10.2174/138161210794454969 PMID: 21158725

[21] Kim, Y.W.; Byzova, T.V. Oxidative stress in angiogenesis and vascular disease. *Blood,* **2014**, *123*(5), 625-631.
http://dx.doi.org/10.1182/blood-2013-09-512749 PMID: 24300855

[22] Raj, S.; Khurana, S.; Choudhari, R.; Kesari, K.K.; Kamal, M.A.; Garg, N.; Ruokolainen, J.; Das, B.C.; Kumar, D. Specific targeting cancer cells with nanoparticles and drug delivery in cancer therapy. *Semin. Cancer Biol.,* **2021**, *69*, 166-177.
http://dx.doi.org/10.1016/j.semcancer.2019.11.002 PMID: 31715247

[23] Gagliardi, A.; Giuliano, E.; Venkateswararao, E.; Fresta, M.; Bulotta, S.; Awasthi, V.; Cosco, D. Biodegradable polymeric nanoparticles for drug delivery to solid tumors. *Front. Pharmacol.,* **2021**, *12*, 601626.
http://dx.doi.org/10.3389/fphar.2021.601626 PMID: 33613290

[24] Venkatraman, S.S.; Ma, L.L.; Natarajan, J.V.; Chattopadhyay, S. Polymer- and liposome-based nanoparticles in targeted drug delivery. *Front. Biosci.,* **2010**, *2*(3), 801-814.
http://dx.doi.org/10.2741/s103 PMID: 20515826

[25] Goodall, S.; Jones, M.L.; Mahler, S. Monoclonal antibody-targeted polymeric nanoparticles for cancer therapy-future prospects. *J. Chem. Technol. Biotechnol.,* **2015**, *90*(7), 1169-1176.
http://dx.doi.org/10.1002/jctb.4555

[26] Sarcan, E.T.; Silindir-Gunay, M.; Ozer, A.Y. Theranostic polymeric nanoparticles for NIR imaging and photodynamic therapy. *Int. J. Pharm.,* **2018**, *551*(1-2), 329-338.
http://dx.doi.org/10.1016/j.ijpharm.2018.09.019 PMID: 30244148

[27] Cruz, L.J.; van Dijk, T.; Vepris, O.; Li, T.M.W.Y.; Schomann, T.; Baldazzi, F.; Kurita, R.; Nakamura, Y.; Grosveld, F.; Philipsen, S.; Eich, C. PLGA-nanoparticles for intracellular delivery of the CRISPR-complex to elevate fetal globin expression in erythroid cells. *Biomaterials,* **2021**, *268*, 120580.
http://dx.doi.org/10.1016/j.biomaterials.2020.120580 PMID: 33321292

[28] Oizumi, I.; Hamai, R.; Shiwaku, Y.; Mori, Y.; Anada, T.; Baba, K.; Miyatake, N.; Hamada, S.; Tsuchiya, K.; Nishimura, S.; Itoi, E.; Suzuki, O. Impact of simultaneous hydrolysis of OCP and PLGA on bone induction of a PLGA-OCP composite scaffold in a rat femoral defect. *Acta Biomater.,* **2021**, *124*, 358-373.
http://dx.doi.org/10.1016/j.actbio.2021.01.048 PMID: 33556607

[29] Tsai, I.L.; Tsai, C.Y.; Kuo, L.L.; Woung, L.C.; Ku, R.Y.; Cheng, Y.H. PLGA nanoparticles containing Lingzhi extracts rescue corneal epithelial cells from oxidative damage. *Exp. Eye Res.,* **2021**, *206*, 108539.
http://dx.doi.org/10.1016/j.exer.2021.108539 PMID: 33741324

[30] Gebreel, R.M.; Edris, N.A.; Elmofty, H.M.; Tadros, M.I.; El-Nabarawi, M.A.; Hassan, D.H. Development and characterization of PLGA nanoparticle-laden hydrogels for sustained ocular delivery of norfloxacin in the treatment of *Pseudomonas* keratitis: An experimental study. *Drug Des. Devel. Ther.,* **2021**, *15*, 399-418.
http://dx.doi.org/10.2147/DDDT.S293127 PMID: 33584095

[31] Raza, A.; Miles, J.A.; Sime, F.B.; Ross, B.P.; Roberts, J.A.; Popat, A.; Kumeria, T.; Falconer, J.R. PLGA encapsulated γ-cyclodextrin-meropenem inclusion complex formulation for oral delivery. *Int. J. Pharm.,* **2021**, *597*, 120280.
http://dx.doi.org/10.1016/j.ijpharm.2021.120280 PMID: 33540004

[32] Tripathi, S.K.; Patel, B.; Shukla, S.; Pachouri, C.; Pathak, S.; Pandey, A. Donepezil loaded PLGA nanoparticles, from modified nano-precipitation, an advanced drug delivery system to treat Alzheimer disease. *J. Phys. Conf. Ser.,* **2021**, *1849*(1), 012001.
http://dx.doi.org/10.1088/1742-6596/1849/1/012001

[33] Shahin, H.; Vinjamuri, B.P.; Mahmoud, A.A.; Mansour, S.M.; Chougule, M.B.; Chablani, L. Formulation and optimization of sildenafil citrate-loaded PLGA large porous microparticles using spray freeze-drying technique: A factorial design and *in-vivo* pharmacokinetic study. *Int. J. Pharm.,* **2021**, *597*, 120320.
http://dx.doi.org/10.1016/j.ijpharm.2021.120320 PMID: 33539999

[34] Shah, P.; Sarolia, J.; Vyas, B.; Wagh, P.; Ankur, K.; Kumar, M.A. PLGA nanoparticles for nose to brain delivery of Clonazepam: Formulation, optimization by 32 Factorial design, *in vitro* and *in vivo* evaluation. *Curr. Drug Deliv.,* **2021**, *18*(6), 805-824.
http://dx.doi.org/10.2174/18755704MTA3lOTgqw
PMID: 32640955

[35] Du, X.; Xue, J.; Jiang, M.; Lin, S.; Huang, Y.; Deng, K.; Shu, L.; Xu, H.; Li, Z.; Yao, J.; Chen, S.; Shen, Z.; Feng, G. A multiepitope peptide, rOmp22, encapsulated in chitosan-PLGA nanoparticles as a candidate vaccine against *Acinetobacter baumannii* infection. *Int. J. Nanomedic.,* **2021**, *16*, 1819-1836.
http://dx.doi.org/10.2147/IJN.S296527 PMID: 33707942

[36] Boroumand, H.; Badie, F.; Mazaheri, S.; Seyedi, Z.S.; Nahand, J.S.; Nejati, M.; Baghi, H.B.; Abbasi-Kolli, M.; Badehnoosh, B.; Ghandali, M.; Hamblin, M.R.; Mirzaei, H. Chitosan-based nanoparticles against viral infections. *Front. Cell. Infect. Microbiol.,* **2021**, *11*, 643953.
http://dx.doi.org/10.3389/fcimb.2021.643953 PMID: 33816349

[37] Kurakula, M.; Raghavendra Naveen, N. Electrospraying: A facile technology unfolding the chitosan based drug delivery and biomedical applications. *Eur. Polym. J.,* **2021**, *147*, 110326.
http://dx.doi.org/10.1016/j.eurpolymj.2021.110326

[38] Li, C.; Fang, K.; He, W.; Li, K.; Jiang, Y.; Li, J. Evaluation of chitosan-ferulic acid microcapsules for sustained drug delivery: Synthesis, characterizations, and release kinetics *in vitro*. *J. Mol. Struct.,* **2021**, *1227*, 129353.
http://dx.doi.org/10.1016/j.molstruc.2020.129353

[39] Shakeran, Z.; Keyhanfar, M.; Varshosaz, J.; Sutherland, D.S. Biodegradable nanocarriers based on chitosan-modified mesoporous silica nanoparticles for delivery of methotrexate for application in breast cancer treatment. *Mater. Sci. Eng. C,* **2021**, *118*, 111526.
http://dx.doi.org/10.1016/j.msec.2020.111526 PMID: 33255079

[40] Zhang, J.; Sun, H.; Gao, C.; Wang, Y.; Cheng, X.; Yang, Y.; Gou, Q.; Lei, L.; Chen, Y.; Wang, X.; Zou, Q.; Gu, J. Development of a chitosan-modified PLGA nanoparticle vaccine for protection against *Escherichia coli* K1 caused meningitis in mice. *J. Nanobiotechnol.,* **2021**, *19*(1), 69.
http://dx.doi.org/10.1186/s12951-021-00812-9 PMID: 33673858

[41] Alshehri, S.; Imam, S.S.; Rizwanullah, M.; Fakhri, K.U.; Rizvi, M.M.A.; Mahdi, W.; Kazi, M.; Kazi, M. Effect of chitosan coating on PLGA Nanoparticles for oral delivery of thymoquinone: *In vitro*, *ex vivo*, and cancer cell line assessments. *Coatings,* **2020**, *11*(1), 6.
http://dx.doi.org/10.3390/coatings11010006

[42] Takeuchi, I.; Suzuki, T.; Makino, K.; Makino, K. Iontophoretic transdermal delivery using chitosan-coated PLGA nanoparticles for transcutaneous immunization. *Colloids Surf. A Physicochem. Eng. Asp.,* **2021**, *608*, 125607.
http://dx.doi.org/10.1016/j.colsurfa.2020.125607 PMID: 29017147

[43] Bruijnincx, P.C.A.; Sadler, P.J. New trends for metal complexes with anticancer activity. *Curr. Opin. Chem. Biol.,* **2008**, *12*(2), 197-206.
http://dx.doi.org/10.1016/j.cbpa.2007.11.013 PMID: 18155674

[44] Frezza, M.; Hindo, S.; Chen, D.; Davenport, A.; Schmitt, S.; Tomco, D.; Ping Dou, Q. Novel metals and metal complexes as platforms for cancer therapy. *Curr. Pharm. Des.,* **2010**, *16*(16), 1813-1825.
http://dx.doi.org/10.2174/138161210791209009 PMID: 20337575

[45] Ikitimur-Armutak, E.I.; Gurel-Gurevin, E.; Kiyan, H.T.; Aydinlik, S.; Yilmaz, V.T.; Dimas, K.; Ulukaya, E. Anti-angiogenic effect of a Palladium(II)-saccharinate complex of terpyridine *in vitro* and *in vivo*. *Microvasc. Res.,* **2017**, *109*, 26-33.
http://dx.doi.org/10.1016/j.mvr.2016.09.002 PMID: 27613574

[46] Meghdadi, S.; Amirnasr, M.; Kiani, M.; Fadaei Tirani, F.; Bagheri, M.; Schenk, K.J. Benign synthesis of quinolinecarboxamide ligands, H_2 bqbenzo and H_2 bqb and their Pd(II) complexes: X-ray crystal structure, electrochemical and antibacterial studies. *J. Coord. Chem.,* **2017**, *70*(14), 2409-2424.
http://dx.doi.org/10.1080/00958972.2017.1336231

[47] Schulz, J.; Renfrew, A.K.; Císařová, I.; Dyson, P.J.; Štěpnička, P. Synthesis and anticancer activity of chalcogenide derivatives and platinum(II) and palladium(II) complexes derived from a polar ferrocene phosphanyl-carboxamide. *Appl. Organomet. Chem.,* **2010**, *24*(5), n/a. p. 392-397.
http://dx.doi.org/10.1002/aoc.1626

[48] Sheldrick, G.M. *SHELXT*-Integrated space-group and crystal-structure determination. *Acta Crystallogr. A Found. Adv.,* **2015**, *71*(1), 3-8.
http://dx.doi.org/10.1107/S2053273314026370 PMID: 25537383

[49] Sheldrick, G.M. Crystal structure refinement with *SHELXL*. *Acta Crystallogr. C Struct. Chem.,* **2015**, *71*(1), 3-8.
http://dx.doi.org/10.1107/S2053229614024218 PMID: 25567568

[50] Sheldrick, G.M. A short history of *SHELX*. *Acta Crystallogr. A,* **2008**, *64*(1), 112-122.
http://dx.doi.org/10.1107/S0108767307043930 PMID: 18156677

[51] Macrae, C.F.; Edgington, P.R.; McCabe, P.; Pidcock, E.; Shields, G.P.; Taylor, R.; Towler, M.; van de Streek, J. Mercury : Visualization and analysis of crystal structures. *J. Appl. Cryst.,* **2006**, *39*(3), 453-457.
http://dx.doi.org/10.1107/S002188980600731X

[52] Mahajan, H.D.; Dayaram Wagh, R.; Baviskar, D.T. Development and evaluation of acyclovir loaded poly lactic-Co-glycolic acid nanoparticles for ocular drug delivery. *Int. J. Pharm. Investig.,* **2021**, *11*(1), 63-68.
http://dx.doi.org/10.5530/ijpi.2021.1.12

[53] Holgado, M.A.; Martin-banderas, ; Alvarez-fuentes, ; Duran-lobato, ; Prados, J.; Melguizo, F. Cannabinoid derivate-loaded PLGA nanocarriers for oral administration: Formulation, characterization, and cytotoxicity studies. *Int. J. Nanomedic.,* **2012**, *7*, 5793-5806.
http://dx.doi.org/10.2147/IJN.S34633 PMID: 23209365

[54] Öztürk, A.A.; Yenilmez, E.; Özarda, M.G. Clarithromycin-loaded poly (lactic-co-glycolic acid) (PLGA) nanoparticles for oral administration: Effect of polymer molecularweight and surface modification with chitosan on formulation, nanoparticle characterization and antibacterial Effects. *Polymers,* **2019**, *11*(10), 1632.
http://dx.doi.org/10.3390/polym11101632 PMID: 31600969

[55] Raheem, S.S.; Hasan, H.F. Preparation of poly(lactic-co-glycolic acid)-loaded pentoxyfilline by nanoparticipation technique. *Med. J. Babylon,* **2021**, *18*(1), 12-17.

[56] Errico, C.; Bartoli, C.; Chiellini, F.; Chiellini, E. Poly(hydroxyalkanoates)-based polymeric nanoparticles for drug delivery. *J. Biomed. Biotechnol.,* **2009**, *2009*, 571702.
http://dx.doi.org/10.1155/2009/571702 PMID: 19789653

[57] Lima, I.A.; Khalil, N.M.; Tominaga, T.T.; Lechanteur, A.; Sarmento, B.; Mainardes, R.M. Mucoadhesive chitosan-coated PLGA nanoparticles for oral delivery of ferulic acid. *Artif. Cells Nanomed. Biotechnol.,* **2018**, *46*(Suppl. 2), 993-1002.
http://dx.doi.org/10.1080/21691401.2018.1477788 PMID: 29842790

[58] Durán-Lobato, M.; Martín-Banderas, L.; Gonçalves, L.M.D.; Fernández-Arévalo, M.; Almeida, A.J. Comparative study of chitosan- and PEG-coated lipid and PLGA nanoparticles as oral delivery systems for cannabinoids. *J. Nanopart. Res.,* **2015**, *17*(2), 61.
http://dx.doi.org/10.1007/s11051-015-2875-y

[59] Khan, N.; Ameeduzzafar, ; Khanna, K.; Bhatnagar, A.; Ahmad, F.J.; Ali, A. Chitosan coated PLGA nanoparticles amplify the ocular hypotensive effect of forskolin: Statistical design, characterization and *in vivo* studies. *Int. J. Biol. Macromol.,* **2018**, *116*, 648-663.
http://dx.doi.org/10.1016/j.ijbiomac.2018.04.122 PMID: 29723623

[60] Zevallos Torres, L.A.; Woiciechowski, A.L.; Oliveira de Andrade Tanobe, V.; Zandoná Filho, A.; Alves de Freitas, R.; Noseda, M.D.; Saito Szameitat, E.; Faulds, C.; Coutinho, P.; Bertrand, E.; Soccol, C.R. Lignin from oil palm empty fruit bunches: Characterization, biological activities and application in green synthesis of silver nanoparticles. *Int. J. Biol. Macromol.,* **2021**, *167*, 1499-1507.
http://dx.doi.org/10.1016/j.ijbiomac.2020.11.104 PMID: 33212110

[61] Yunita, E.; Yulianto, D.; Fatimah, S.; Firanita, T. Validation of UV-Vis spectrophotometric method of quercetin in ethanol extract of tamarind Leaf. *J. Fund. Appl. Pharmaceutic. Sci.,* **2020**, *1*(1), 11-18.
http://dx.doi.org/10.18196/jfaps.010102

[62] Öztürk, A.A.; Güven, U.M.; Yenilmez, E. Flurbiprofen loaded gel based topical delivery system: Formulation and *in vitro* characterization with new developed UPLC method. *ACTA Pharmaceutic. Sci.,* **2018**, *56*(4), 81-105.
http://dx.doi.org/10.23893/1307-2080.APS.05627

[63] Öztürk, A.A.; Güven, U.M. Cefaclor monohydrate loaded microemulsion formulation for topical application: Characterization with new developed UPLC method and stability study. *J. Res. Pharm.,* **2019**, *23*(3), 426-440.
http://dx.doi.org/10.12991/jrp.2019.150

[64] Singh, S.K.; Girotra, P.; Gupta, S. Targeting silymarin for improved hepatoprotective activity through chitosan nanoparticles. *Int. J. Pharm. Investig.,* **2014**, *4*(4), 156-163.
http://dx.doi.org/10.4103/2230-973X.143113 PMID: 25426436

[65] El-Nahas, A.E.; Allam, A.N.; Abdelmonsif, D.A.; El-Kamel, A.H. Silymarin-loaded eudragit nanoparticles: Formulation, characterization, and hepatoprotective and toxicity evaluation. *AAPS Pharm. Sci. Tech.,* **2017**, *18*(8), 3076-3086.
http://dx.doi.org/10.1208/s12249-017-0799-9 PMID: 28516410

[66] Brand-Williams, W.; Cuvelier, M.E.; Berset, C. Use of a free radical method to evaluate antioxidant activity. *Lebensm. Wiss. Technol.,* **1995**, *28*(1), 25-30.
http://dx.doi.org/10.1016/S0023-6438(95)80008-5

[67] Vinderola, C.G.; Reinheimer, J.A. Culture media for the enumeration of *Bifidobacterium bifidum* and *Lactobacillus acidophilus* in the presence of yogurt bacteria. *Int. Dairy J.,* **1999**, *9*(8), 497-505.
http://dx.doi.org/10.1016/S0958-6946(99)00120-X

[68] Boorn, K.L.; Khor, Y.Y.; Sweetman, E.; Tan, F.; Heard, T.A.; Hammer, K.A. Antimicrobial activity of honey from the stingless bee *Trigona carbonaria* determined by agar diffusion, agar dilution, broth microdilution and time-kill methodology. *J. Appl. Microbiol.,* **2010**, *108*(5), 1534-1543.
http://dx.doi.org/10.1111/j.1365-2672.2009.04552.x PMID: 19811569

[69] CLSI. *Methods for Dilution Antimicrobial Susceptibility Tests or Bacteria That Grow Aerobically; Approved St andard,* 9th ed; Clinical and Laboratory Standards Institute: Wayne, PA, **2012**.

[70] Weinstein, M.P.; Lewis, J.S. II The clinical and laboratory standards institute subcommittee on antimicrobial susceptibility testing: background, organization, functions, and processes. *J. Clin. Microbiol.,* **2020**, *58*(3), e01864-19.
http://dx.doi.org/10.1128/JCM.01864-19 PMID: 31915289

[71] Mota, C.R.A.; Miranda, K.C.; Lemos, J.A.; Costa, C.R.; Souza, L.K.H.; Passos, X.S.; Silva, H.M.; Silva, M.R.R. Comparison of *in vitro* activity of five antifungal agents against dermatophytes, using the agar dilution and broth microdilution methods. *Rev. Soc. Bras. Med. Trop.,* **2009**, *42*(3), 250-254.
http://dx.doi.org/10.1590/S0037-86822009000300003 PMID: 19684970

[72] Kıyan, H.T.; Demirci, B.; Başer, K.H.C.; Demirci, F. The *in vivo* evaluation of anti-angiogenic effects of *Hypericum* essential oils using the chorioallantoic membrane assay. *Pharm. Biol.,* **2014**, *52*(1), 44-50.
http://dx.doi.org/10.3109/13880209.2013.810647 PMID: 24044783

[73] Singh, J.; Deb, M.; Elias, A.J. Palladacycles based on 8-aminoquinoline carboxamides of cobalt and iron sandwich compounds and a new method to α-alkylate Cp rings of metal sandwich carboxamides. *Organometallics,* **2015**, *34*(20), 4946-4951.
http://dx.doi.org/10.1021/acs.organomet.5b00504

[74] Mukherjee, T.; Sen, B.; Zangrando, E.; Hundal, G.; Chattopadhyay, B.; Chattopadhyay, P. Palladium(II) and platinum(II) complexes of deprotonated N,N′-bis(2-pyridinecarboxamide)-1,2-benzene: Synthesis, structural characterization and binding interactions with DNA and BSA. *Inorg. Chim. Acta,* **2013**, *406*, 176-183. http://dx.doi.org/10.1016/j.ica.2013.04.033

[75] Navrátil, M.; Císařová, I.; Alemayehu, A.; Škoch, K.; Štěpnička, P. Synthesis and structural characterisation of an *N* -Phosphanyl ferrocene carboxamide and its ruthenium, rhodium and palladium complexes. *Chem. Plus. Chem.,* **2020**, *85*(6), 1325-1338. http://dx.doi.org/10.1002/cplu.202000303 PMID: 32567813

[76] Şenel, B.; Öztürk, A.A. New approaches to tumor therapy with siRNA-decorated and chitosan-modified PLGA nanoparticles. *Drug Dev. Ind. Pharm.,* **2019**, *45*(11), 1835-1848. http://dx.doi.org/10.1080/03639045.2019.1665061 PMID: 31491363

[77] Zirak, M.B.; Pezeshki, A. Effect of surfactant concentration on the particle size, stability and potential zeta of beta carotene nano lipid carrier. *Int. J. Curr. Microbiol. Appl. Sci.,* **2015**, *4*(9), 924-932.

[78] Öztürk, A.A.; Aygül, A.; Şenel, B. Influence of glyceryl behenate, tripalmitin and stearic acid on the properties of clarithromycin incorporated solid lipid nanoparticles (SLNs): Formulation, characterization, antibacterial activity and cytotoxicity. *J. Drug Deliv. Sci. Technol.,* **2019**, *54*, 101240. http://dx.doi.org/10.1016/j.jddst.2019.101240

[79] Emami, J.; Mohiti, H.; Hamishehkar, H.; Varshosaz, J. Formulation and optimization of solid lipid nanoparticle formulation for pulmonary delivery of budesonide using Taguchi and Box-Behnken design. *Res. Pharm. Sci.,* **2015**, *10*(1), 17-33. PMID: 26430454

[80] Müller, R.H.; Mäder, K.; Gohla, S. Solid lipid nanoparticles (SLN) for controlled drug delivery-a review of the state of the art. *Eur. J. Pharm. Biopharm.,* **2000**, *50*(1), 161-177. http://dx.doi.org/10.1016/S0939-6411(00)00087-4 PMID: 10840199

[81] Chronopoulou, L.; Massimi, M.; Giardi, M.F.; Cametti, C.; Devirgiliis, L.C.; Dentini, M.; Palocci, C. Chitosan-coated PLGA nanoparticles: A sustained drug release strategy for cell cultures. *Colloids Surf. B Biointerfaces,* **2013**, *103*, 310-317. http://dx.doi.org/10.1016/j.colsurfb.2012.10.063 PMID: 23261553

[82] Wang, Y.; Li, P.; Kong, L. Chitosan-modified PLGA nanoparticles with versatile surface for improved drug delivery. *AAPS Pharm. Sci. Tech.,* **2013**, *14*(2), 585-592. http://dx.doi.org/10.1208/s12249-013-9943-3 PMID: 23463262

[83] Jayasundara, U.K.; Herath, H.M.M.B.; Kaushalya, P.V.N. Method development, validation, and concentration determination of metformin hydrochloride and atorvastatin calcium using UV-visible spectrophotometry. *J. Anal. Bioanal. Tech.,* **2021**, *12*(2), 428. http://dx.doi.org/10.4172/2155-9872.1000428

[84] Shrestha, S.; Maharjan, S.; Pakhrin, S.; Poudel, A.; Poudel, S.; Thapa, N.; Gaire, A.; Shrestha, J.R. Estimation and validation of methylcobalamin in tablet dosage form using UV-visible spectrophotometric method. *Am. Sci. Res. J. Eng. Technol. Sci.,* **2021**, *77*(1), 220-229.

[85] Lavakumar, S.; Vivekanand, P.A.; Prince, A.A.M. Simultaneous analysis of octylmethoxycinnamate and butylmethoxydibenzoylmethane in sunscreen products by a validated UV-spectrophotometric method. *Mater. Today Proc.,* **2021**, *36*, 893-897. http://dx.doi.org/10.1016/j.matpr.2020.07.025

[86] Ali, M.S.; Elsaman, T. Development and validation of the UV spectrophotometric method for simultaneous determination of paracetamol and pseudoephedrine in bulk and combined tablet dosage form. *Pharm. Chem. J.,* **2021**, *54*(12), 1306-1310. http://dx.doi.org/10.1007/s11094-021-02360-w

[87] Shen, S.; Wu, Y.; Liu, Y.; Wu, D. High drug-loading nanomedicines: Progress, current status, and prospects. *Int. J. Nanomedic.,* **2017**, *12*, 4085-4109. http://dx.doi.org/10.2147/IJN.S132780 PMID: 28615938

[88] Parveen, S.; Sahoo, S.K. Long circulating chitosan/PEG blended PLGA nanoparticle for tumor drug delivery. *Eur. J. Pharmacol.,* **2011**, *670*(2-3), 372-383. http://dx.doi.org/10.1016/j.ejphar.2011.09.023 PMID: 21951969

DISCLAIMER: The above article has been published, as is, ahead-of-print, to provide early visibility but is not the final version. Major publication processes like copyediting, proofing, typesetting and further review are still to be done and may lead to changes in the final published version, if it is eventually published. All legal disclaimers that apply to the final published article also apply to this ahead-of-print version.